Electrogasdynamic Power Generation

BERNARD KAHN* AND MEREDITH C. GOURDINE†
Curtiss-Wright Corporation, Wood-Ridge, N. J.

A basic theoretical and experimental study of electrogasdynamic power generation is presented. A "slender-channel" model is analyzed, and the results of an experimental program designed to determine the feasibility of this model are presented. The experimental results on a dielectric slender-channel generator have led to further theoretical and experimental investigations on a segmented slender-channel model. Experimental results show good correlation with the theory. The results suggest the use of colloidal ions in further investigations of this technique for power generation.

Nomenclature

E_a = electric field at attractor, v/m
E_b = breakdown field strength between parallel electrodes, v/m
p = pressure drop, newtons/m^2
E_r = radial electric field, v/m
E_x = axial electric field, v/m
r = radial distance, m
x = axial distance, m
n_i = ion concentration, ions/m^3
e = electron charge, 1.6×10^{-19} coul
ϵ_0 = permittivity of free space, 8.85×10^{-12} farads/m
f = force per unit volume, newtons/m^3
F = total force, newtons
F/A = specific force, newtons/m^2
I_n = needle current, amp
I_a = attractor current, amp
I_c = collector current, amp
J = current density, amp/m^2
K_i = mobility of ions, m^2/v-sec
λ = channel charge parameter, m
P = power, w
u = velocity, m/sec

1. Introduction

SEVERAL investigations[1–4] have concerned themselves with the feasibility of converting flow kinetic energy into high-voltage, low-current electricity by electrogasdynamic (EGD) techniques. EGD is the study of the interactions between an electrostatic field and the flow of a dielectric gas containing a small percentage of unipolar ions. Recently,

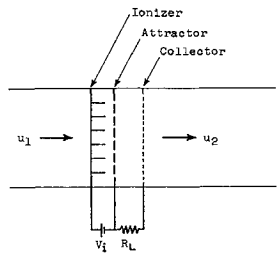

Fig. 1 Broad-channel EGD converter.

Received July 22, 1963; revision received April 9, 1964. This research was supported by the U. S. Air Force, Aerospace Research Laboratories, Wright-Patterson Air Force Base, Ohio, under Contract AF33(657)-10832. The authors wish to express their appreciation to M. P. Khan, J. DelGuidice, and D. Lalas for their cooperation in this program. J. Tiddes offered valuable technical assistance in the laboratory.

* Project Manager, Advanced Energy Conversion Department, Wright Aeronautical Division. Member AIAA.
† Formerly Chief Scientist, Wright Aeronautical Division. Associate Fellow Member AIAA.

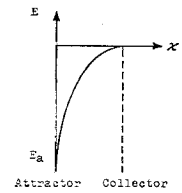

Fig. 2 Field distribution in a broad-channel converter.

Lawson, Von Ohain, and Wattendorf[5] reported on the feasibility of multistaging many EGD converters of the broad-channel type shown in Fig. 1. Multistaging is required because the pressure drop per stage is $\Delta p = \epsilon_0 E_a^2/2$, and E_a is limited by the breakdown field strength E_b between parallel electrodes (at standard temperature and pressure, $E_b = 3 \times 10^6$ v/m), where E_a is the negative electric field at the attractor (Fig. 2). Therefore, the maximum pressure drop per stage would be

$$\Delta p_{\max} \approx \epsilon_0 E_0^2/2 \approx 39.9 \text{ newtons/m}^2 = 3.99 \times 10^{-4} \text{ atm}$$

Thus, for practical applications in a closed-loop generator, hundreds or thousands of stages would be necessary. Nevertheless, Lawson et al.[5] show that multistaging may still be feasible in very high-pressure systems where E_b is much larger than at standard temperature and pressure.

In the slender-channel geometry, the maximum pressure drop becomes

$$\Delta p_{\max} = \epsilon_0 E_x E_r^* \, 2L/R$$

The radial component of the electric field E_r^* can be much higher without suffering breakdown because of the dielectric wall. For Mylar, for instance, E_r^* can be as high as 10^8 v/m. This should result in an improvement of at least two orders of magnitude before considering that $2L/R > 1$ in the slender-channel configuration.

In an attempt to avoid multistaging and simplify EGD energy conversion, the authors have considered the slender-channel model illustrated in Fig. 3 where the distance between attractor and collector is large compared to the diameter. Two slender-channel models are considered in this report: the dielectric slender channel and the segmented slender channel.

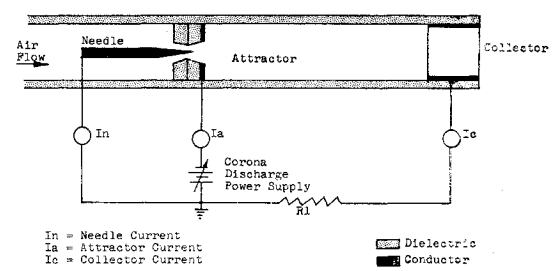

Fig. 3 Single-needle dielectric slender-channel generator.

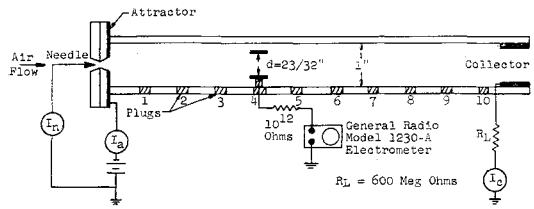

Fig. 4 Probe 4 measuring electric potential at station 4.

2. Dielectric Slender Channel

2.1 Theory

In analyzing broad-channel models, the assumption is made that derivatives in the transverse direction are small compared to derivatives in the axial direction; therefore, it seems reasonable to reverse this assumption in analyzing the slender-channel model and to approximate Poisson's equation by

$$(1/r)(\partial/\partial r)rE_r \approx (e/\epsilon_0)n_i$$

Upon integration, we get the radial electric field at the tube wall E_r^*, i.e.,

$$E_r^*(x) = \frac{e}{\epsilon_0}\frac{1}{R}\int_0^R n_i(r, x)rdr = \frac{e}{\epsilon_0}n_i(x)\frac{R}{2} \quad (1)$$

where $n_i(x)$ is the mean ion concentration at a given station x along the channel.

The force per unit volume on the gas is, from Eq. (1),

$$f_x = eE_x n_i = eE_x(2\epsilon_0/Re) = (\epsilon_0 E_x E_r^*)(2/R)$$

Assuming that E_x and E_r^* are constants, then the net force on the gas is

$$F_x = f_x \pi R^2 L = (\epsilon_0 E_x E_r^*)2\pi RL$$

This means that the net force on the gas is the sum of the Maxwell shear stresses $\epsilon_0 E_x E_r^*$ on the dielectric tube wall of area $2\pi RL$. This statement can be proved true even if we do not assume that E_x and E_r^* are constants. The pressure drop in a single stage is

$$F_x/\pi R^2 = \Delta p = (\epsilon_0 E_x E_r^*)(2L/R)$$

Since neither E_x nor E_r^* is limited by the breakdown field between parallel plate electrodes, the Maxwell shear stress $\epsilon_0 E_x E_r^*$ in the slender channel can be made much larger than the Maxwell normal stress $\epsilon_0 E_x^2$ in the broad channel, and,

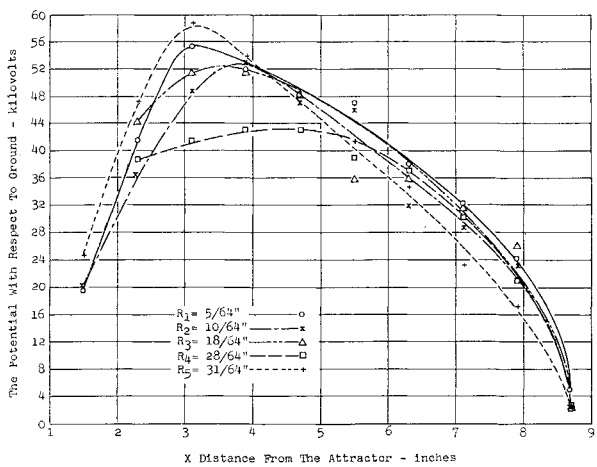

Fig. 5 The potential distribution in the channel.

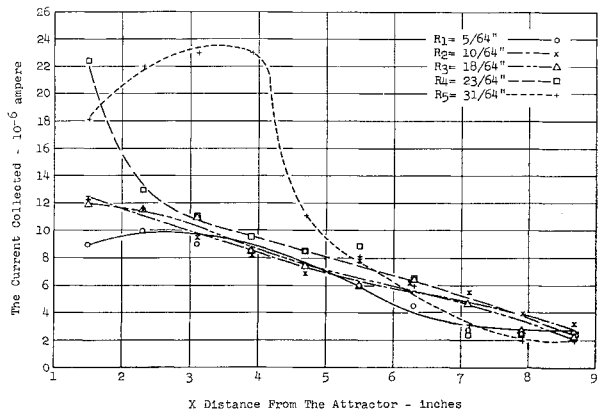

Fig. 6 The current distribution in the channel.

in addition, there is the factor $2L/R \gg 1$ that helps to make much larger pressure drops attainable in a single stage. This is the primary motivation for studying the slender channel. Experiments indicate that the theory appears to be accurate up to a point downstream in the channel. The effect of space charge causing the relatively high-mobility ions of air to deposit on the walls of the channel was not predicted. The theory was then modified to include this phenomenon, as described later.

2.2 Dielectric Slender Channel: Experiments

For experimental evaluation, the models used incorporated corona discharge points as generators of unipolar ions. This type of generator has been used in previous experimental studies.[6-8]

In this approach, the simple model (Fig. 3) incorporates a single needle, which was found to produce adequate ions and to give more flexible control than multipoint ion generators.

The dielectric model was used to investigate a number of parameters of the EGD generator. These included the investigation of the axial electric field E_x, the radial electric field E_r, the current distribution, ion concentration, and power density in the channel.

In order to examine the electric field and current distribution in the channel, a series of copper rings of different diameters was inserted individually at various stations in the channel. Both potential and current data were taken at various stations in the channel. In order to examine the potential at any point in the channel, it is essential to extract virtually no current from the flow while making the measurement. The potential measuring device used was a General Radio model 1230-A electrometer with a calibrated 10^{12}-ohm multiplier. A typical probe measurement is shown in Fig. 4. The results of the probing of the channel are given

Table 1 Collector currents as a function of collector position

Distance from collector to attractor, in.	Needle current (I_n), amp $\times 10^{-6}$	Attractor current (I_a), amp $\times 10^{-6}$	Collector current (I_c), amp $\times 10^{-6}$
1.50	40.0	25.0	15.0
2.25	40.0	28.0	12.0
3.00	40.0	34.0	7.5[a]
3.75	40.0	35.0	4.8
4.50	40.0	37.0	3.6[a]
5.25	40.0	37.5	2.5
6.00	40.0	38.0	2.0
6.75	40.0	38.0	1.5
7.50	40.0	38.5	1.0
8.25	40.0	40.0	

[a] Discrepancy due to reading error.

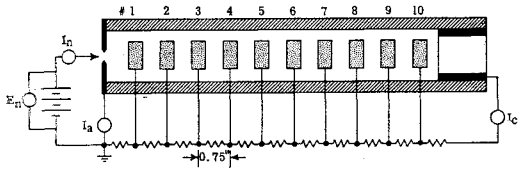

Fig. 7 Ion flow control experiment.

in Fig. 5, which is a plot of the potential, and Fig. 6, which is a plot of the current vs the distance from the attractor.

Another experiment was run to establish how the currents were behaving in the channel. In this case, the collector was moved to various axial stations, and the resulting needle, attractor, and collector currents were observed. Table 1 gives these currents as a function of the collector position.

An experiment in which control of the axial electric field was attempted is illustrated in Fig. 7. The brass rings at the various stations were as heavily insulated as possible. The purpose of the rings was to confine the ion flow to the region inside the rings and to prevent them from migrating into the boundary layer on the walls of the dielectric channel. At the high electrostatic potentials that were generated at the rings, it was found impossible to prevent them from collecting currents and upsetting the load field. When all of the rings were tied together and left floating, it was noted that the potential at the collector downstream rose by a factor of eight. This indicated that more ions had been channeled downstream and that an experiment could be devised in which a controlled E_x could be achieved using a segmented slender channel. These experiments are described elsewhere in this paper.

A high-velocity air flow experiment has been run using a supersonic dielectric model. The installation and model are shown in Fig. 8. The model was designed for Mach 2 air flow. In this experiment, 30 kv at 50 μamp have been generated at a collector position 23 in. downstream from the attractor. The wall thickness of the Lucite channel was $\frac{1}{8}$ in., but the experiment was terminated by electric breakdown occurring at a point 14 in. from the attractor. In this experiment, a power density of 11.9 kw/m^2 and an ion concentration of 4×10^{16} ions/m^3 were obtained.

2.3 Conclusions: Dielectric Slender Channel

Figure 5 shows that the potential increases steadily with distance from the attractor, or that E_x is negative and almost uniform up to about 3 in.; then the potential decreases, and the electric field becomes positive. Beyond this point ions are accelerated to the collector, and this is contrary to theoretical predictions. Figure 6 and the data of Table 1 show the reason for this deviation. Ions drift radially toward the wall because of the space-charge-induced radial field; they then get into the boundary layer and are driven back to the attractor by the opposing axial field. It is this deposition of ions on the walls which sets up this unexpected potential distribution. It is important to note that the hump in the potential distribution moved out to 14 in. in the supersonic experiments, compared to only 3 in. in the low-velocity experiments.

Preliminary experiments of the type shown in Fig. 7 showed us that, by properly biasing the channel, the potential distribution could be made linear and E_x could be made negative and uniform all the way down the channel. Further theoretical and experimental studies of biasing lead us to the segmented slender-channel model described below.

3. Segmented Slender Channel

3.1 Theory

In the segmented slender-channel model (Fig. 9), ions reaching the well are drained off through the ring electrodes,

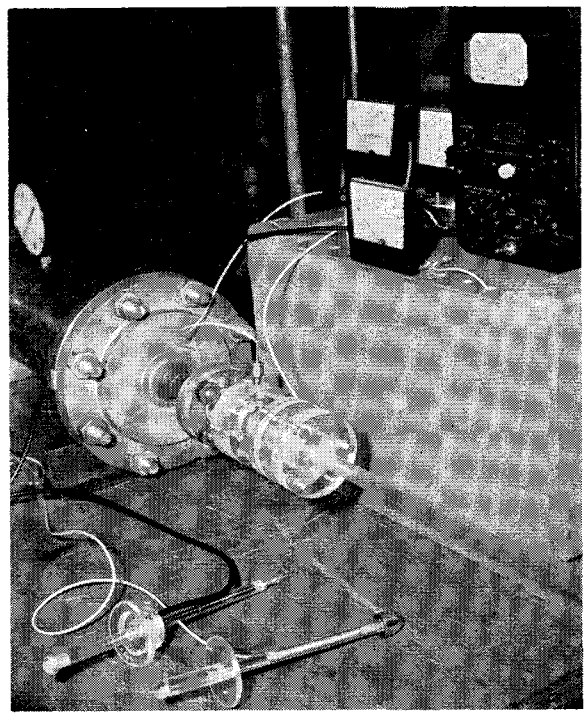

Fig. 8 Supersonic dielectric slender-channel generator.

through the bias resistors, and returned to ground (the attractor). The bias resistors are chosen such that $R_1 < R_2 < R_3$, etc., and the voltage drops between rings are all equal; thus, E_x = const. For this case the body force is given by

$$f = en_iE_x \tag{2}$$

The radial electric field gives the radial current J_r as

$$J_r(r) = en_i(K_iE_r) \tag{3}$$

From continuity of charge,

$$(1/r)(\partial/\partial r)(rJ_r) + (\partial/\partial x)J_x = 0 \tag{4}$$

Integration of (4) from 0 to R gives

$$\pi R^2(\partial J_x/\partial x) = -2\pi Ren_iK_iE_r^*(x) \tag{5}$$

Poisson's equation for this case is simply

$$(1/r)(\partial/\partial r)(rE_r) = en_i/\epsilon_0 \tag{6}$$

Integrating (6) and assuming n_i uniform across the channel, we get

$$E_r^*(x) = (e/\epsilon_0)n_i(x)(R/2) \tag{7}$$

Substituting (7) into (5) and noting that $J_x = en_i(u + K_iE_x)$, we get, after integration,

$$n_i(x)/n_i(0) = 1/[1 + (x/\lambda)] \tag{8}$$

where

$$\lambda \equiv \epsilon_0(u + K_iE_x)^2/K_iJ_x(0)$$

It is interesting to note that the form of the charge distribution of Eq. (8) is the same as obtained by other investigators.[11, 12]

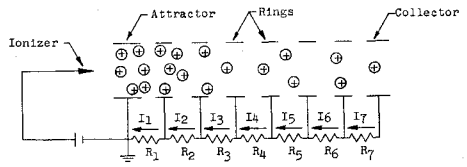

Fig. 9 Schematic diagram of segmented electrode model.

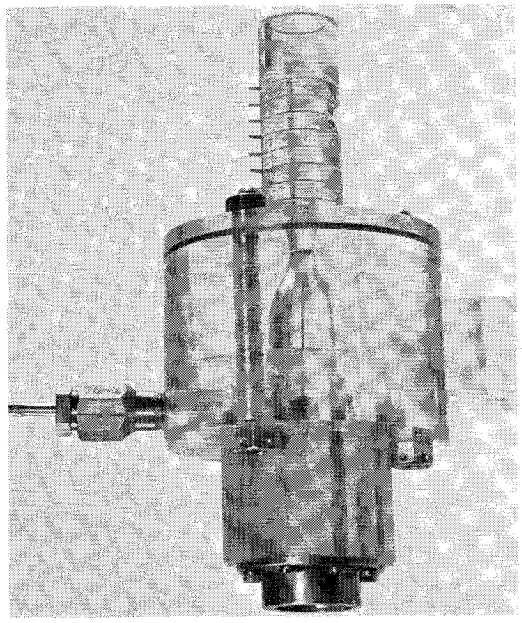

Fig. 10 Segmented electrode field bias model.

The total thrust is given by

$$F = \int_0^x eE_x n_i A\,dx$$

Thus integration gives, for a constant-area channel,

$$F/A = \epsilon_0 E_x[(u/K_i) + E_x] \ln[1 + (x/\lambda)] \tag{9}$$

The condition for maximum force per unit area can be obtained from Eq. (9) as

$$E_x = -\frac{\mu}{2K_i - \{2J_x(0)xK_i^2/\epsilon_0[1 + (x/\lambda)] \ln[1 + (x/\lambda)]\}} \tag{10}$$

The values of the resistances are determined by the equation

$$E_x = -I(dR/dx) = (\pi d^2/4)en_i(u + K_iE_x)(dR/dx)$$

Using (8) and integrating yields the resistance distribution

$$R(x) = [E_x/I_x(0)]x[1 + (x/\lambda)] \tag{11}$$

The power output is given by

$$P = \int_0^{R(x)} I^2(x)dR(x)$$

using (11), the power output is

$$P = E_xI_x(0)\lambda\left[2 \ln\left(1 + \frac{x}{\lambda}\right) - \frac{x/\lambda}{1 + (x/\lambda)}\right] \tag{12}$$

To check the preceding theory, we conducted an experiment in which $I_x(0) = 1 \times 10^{-6}$ amp, $d = \frac{3}{16}$ in., $K_i = 10^{-4}$ m²/v-sec, and $u \approx 100$ m/sec. Making Δx (the spacing between electrodes) of the same order as λ, the uniformity of E_x is guaranteed. The values of the resistance are calculated from (11).

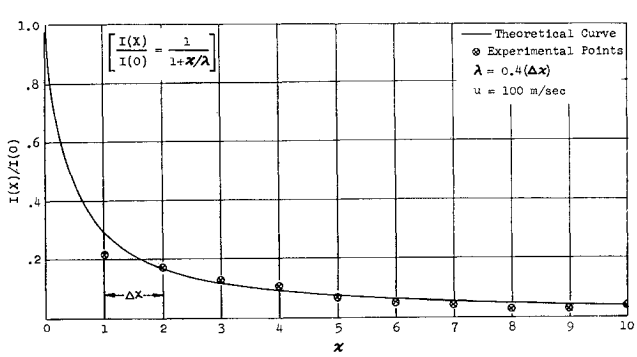

Fig. 11 Theoretical and experimental current distribution in field bias model.

The calculated values of the resistances are

$R_1 = 5.7 \times 10^9\ \Omega$ $R_2 = 12.2 \times 10^9\ \Omega$
$R_3 = 1.8 \times 10^{10}\ \Omega$ $R_4 = 2.5 \times 10^{10}\ \Omega$
$R_5 = 3.1 \times 10^{10}\ \Omega$ $R_6 = 3.8 \times 10^{10}\ \Omega$
$R_7 = 4.2 \times 10^{10}\ \Omega$ $R_8 = 5.2 \times 10^{10}\ \Omega$
$R_9 = 5.8 \times 10^{10}\ \Omega$ $R_{10} = 6.5 \times 10^{10}\ \Omega$

The distance (Δx) between the resistors in the experimental model is 5×10^{-3} m.

3.2 Segmented Slender Channel: Experiments

The segmented slender-channel model is illustrated in Fig. 10. From the electrodynamic analysis, $n_i(x)/n_i(0) = 1/[1 + (x/\lambda)]$. The velocities used in these experiments can be considered constant, and

$$n_i(x)/n_i(0) \approx I(x)/I(0)$$

The currents in each segment of the channel were measured with all of the rest of the segments short-circuited to ground. Figure 11 is a plot of $I(x)/I(0)$ vs x for $\lambda \approx 0.4\Delta x$, where Δx is the spacing between the segmented electrodes. The theoretical and actual values are compared.

From the analysis, values of resistances were computed to establish uniform voltage drops across each segment. These resistors are connected to the segmented electrodes as shown in Fig. 12.

This circuit is used to bias the E_x field uniformly. In addition, since the mobility of the fluid (K_i) is the only parameter that cannot be measured directly, the results of these experiments can be used to determine the mobility of the fluid. The mobility computed from the experimental results was 1.65×10^{-4} m²/v-sec.

The first readings were potential readings taken with the electrometer with the segmented electrodes floating. The results (Fig. 13) are the same as for the dielectric slender channel. The next data taken were electrometer potential readings with the bias resistors connected to the segmented electrodes. It is to be noted that, for the downstream reading, the value of the electrometer multiplier resistance approaches the resistance of the circuit, and the voltages read low due to instrument loading error. To correct this, an attempt was made to read the currents in the various branches, but, with an I_0 of 1 μamp it was difficult to read fractional microampere currents at high potentials with any degree of accuracy, especially in the downstream segments. To alleviate this, the test was run again with a new set of biasing resistors and with $I_0 = 4\mu$ amp. Figure 14 is a plot of the voltage drops vs segment position.

It is felt that the best data were obtained for the condition where the current is read individually in each segment with the rest of the electrodes short-circuited to ground. In this case, the readings are not disturbed by high electrostatic fields. Under these conditions, E_x is close to zero, and $\lambda \approx \epsilon_0 u^2/K_iJ_x(0)$. The mobility can thus be obtained from this directly. The use of such models to monitor mobility is indicated.

The theoretical predictions and the experimental results for the segmented slender channel agree quite well. Difficulties in measuring small currents in high electrostatic fields have been overcome. When the electrodes are shorted to

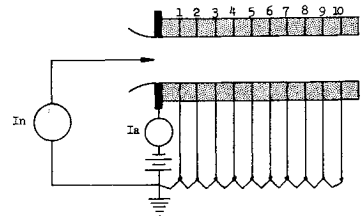

Fig. 12 Schematic diagram of field bias model.

ground, a measurement of the current collected by each electrode determines λ; then a measurement of u and I_0 is sufficient to determine the mobility of the ions quite accurately.

3.3 Losses

In a closed thermodynamic cycle EGD generator system, the magnitude of losses must be considered. The loss due to leakage currents are negligible and are controlled by using shielded wire and proper terminal design. The energy required to produce the corona discharge is very small and can be neglected. In some of the open-cycle experiments that were performed, the system was made regenerative, that is, once started, the ionization power supply was removed, and a portion of the output power of the generator was used to supply the input charged particles.

A major loss factor to be considered is friction, which plays an important role in EGD converters. The conversion efficiency depends mostly on the ratio of frictional force to body force, expressed as

$$\frac{|f_f/f_z|}{1 + |f_f/f_z|}$$

as shown in Ref. 13.

In the broad-channel approach, this ratio is close to unity, and conversion efficiencies are in the order of 0.01 to 0.1%. By a slight improvement in this ratio, e.g., one order of magnitude, the conversion efficiency increases to very attractive values of 30 to 40%. This appears possible because of the larger body forces in slender-channel converters.

4. Conclusions

By using colloidal ions instead of molecular ions, it is possible to reduce the mobility K_i by a factor of 100 or more (see Ref. 3). This would then make the EGD interaction strong and efficient enough to be practical as the energy conversion section of a closed thermodynamic cycle.

To date, attempts to measure pressures in the channel were not successful due to deposition of ions on the channel walls and aerodynamic problems in pressure probing. In the model used in the segmented slender-channel experiments, the diameter of the channel was too small to include pressure probing. The future program includes pressure measurements in a large-scale segmented electrode model.

An investigation involving colloidal ion research has recently been reported.[9] The program described involves a ballistic approach that consists of the acceleration of charged

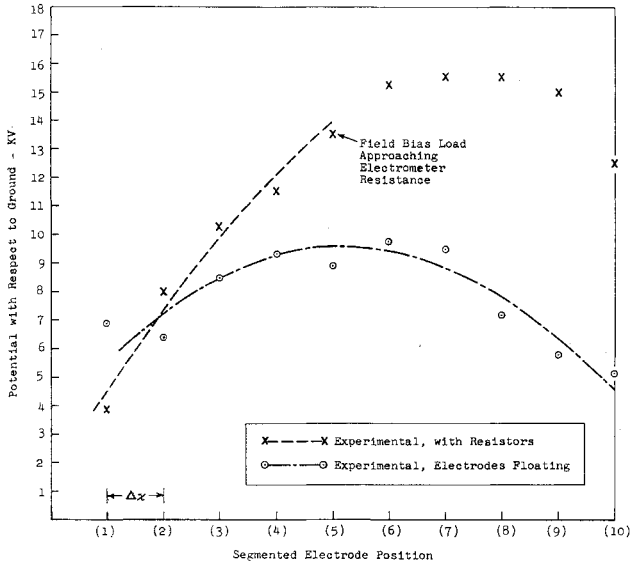

Fig. 13 Measured potential distribution in field bias model.

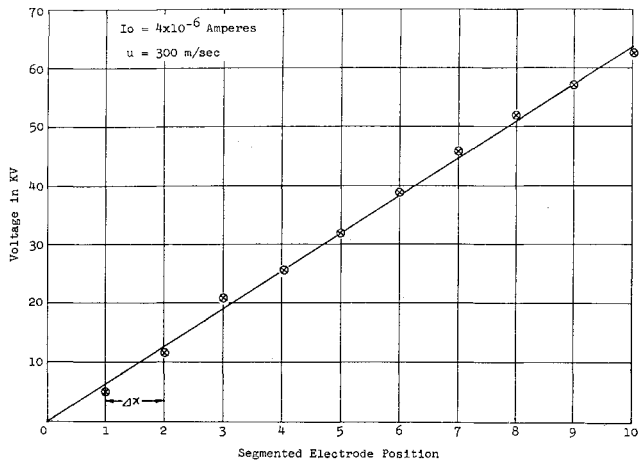

Fig. 14 Potential distribution from current readings in each segment, field bias model.

particles in a vacuum by means of electric fields. Outstanding problems involved in the ballistic approach are the overcoming of Coulomb beam repulsion forces, which in a low-density near-vacuum system must be overcome by electrostatic focusing, and particle collection and recirculation in a closed thermodynamic cycle in which the energy is at very low pressures. The main advantage to this approach is the elimination of multistaging, since high-pressure ratios are predicted.

Our paper concludes that, if colloidal ions can be produced conveniently, they can be transported down a segmented slender channel to produce a strong and efficient EGD interaction with a gas flow. The interaction is stronger and more efficient at higher densities (see Ref. 10) and appears feasible as a direct converter of flow kinetic energy into high-voltage electric power.

References

[1] Bennet, W. E., "The generation of dc at high potentials," Res. Appl. Ind. **12**, 455–459 (December 1959).

[2] Gourdine, M. C., "Power generation by means of the electric wind," TR 32-6, Jet Propulsion Lab., Pasadena, Calif. (April 1960).

[3] Marks, A. M., "Heat-electrical power conversion through the medium of a charged aerosol," Patent 2,638,555 (May 12, 1953).

[4] Sherman, A., Sutton, G. W., Smith, J. M., Von Iwaarden, J., Robben, F. A., Millheim, F., Blecher, S., and Flaherty, T., "Study of electrical energy conversion systems," Aeronautical Systems Div. TR 61-379 (September 1961).

[5] Lawson, M., Von Ohain, H., and Wattendorf, F., "Performance potentialities of direct energy conversion processes between electrostatic and fluid dynamic energy," ARL-178, Aeronautical Research Lab., Office of Aerospace Research, U. S. Air Force (December 1961).

[6] Stuetzer, O. M., "Ion transport high voltage generators," Rev. Sci. Instr. **32**, 16–22 (1961).

[7] Wheeler, H. P., Jr., "The volt-ampere characteristics of an electrohydrodynamic generator," Air Force Institute of Technology Rept. GA/ME/62-8 (August 1962).

[8] Lauritsen, T. N., "Ion production and flow in an electrohydrodynamic generator," Air Force Institute of Technology Rept. GA/ME/62-3 (August 1962).

[9] Cox, A. L., "Colloidal electrohydrodynamic energy converter," AIAA J. **1**, 2491–2497 (1963).

[10] Marks, A., Barreto, E., and Chu, C. K., "Charged aerosol energy converter," AIAA J. **2**, 45–51 (1964).

[11] Foster, W. W., "Deposition of unipolar charged aerosol particles by mutual repulsion," Brit. J. Appl. Phys. **10**, 206 (1959).

[12] Whitby, K. T., "Generator for producing high concentrations of small ions," Rev. Sci. Instr. **32**, 1355 (1961).

[13] Gourdine, M. C., Barreto, E., and Khan, M. P., "On the performance of electrogasdynamic generators," *Proceedings of the Fifth Sgmposium on Engineering Aspects of Magnetohydrodynamics* (April 1–2, 1964).